Electronic Supplementary Material (ESI) for Nanoscale

Electronic Supplementary Information

A chelation-induced cooperative self-assembly methodology for the synthesis of mesoporous metal hydroxide and oxide nanospheres

Yali Ma,[a] Yu Zhang,[c] Xue Wang,[a] Meihong Fan,[a] Kaiqian Li,[a] Tao Wang,[a] Yunling Liu,[a] Qisheng Huo,[a] Zhen-An Qiao[a*] and Sheng Dai[b]

[a] *State Key Laboratory of Inorganic Synthesis and Preparative Chemistry, College of Chemistry, International Joint Research Laboratory of Nano-Micro Architecture Chemistry (NMAC), Jilin University, Changchun, Jilin 130012, P. R. China*

[b] *Chemical Sciences Division, Oak Ridge National Laboratory, Oak Ridge, TN 37831 (USA)*

[c] *Liaoning Key Laboratory for Green Synthesis and Preparative Chemistry of Advanced Materials, College of Chemistry, Liaoning University, Shenyang 110036 (China)*

**Email:* *qiaozhenan@jlu.edu.cn*

Fabrication and characterization of photocurrent experiment. The fabrication of the photoelectrochemical cell was based on a process previously reported.[1] Crystalline ZnO-200-T (T=300, 350, 400, 600°C) nanospheres derived from $Zn(OH)_2$-200 calcinated at different temperatures were dissolved in ethanol under sonication, and a homogenous paste was obtained after a few minutes. Then the paste was held at room temperature under stirring for 12 h. After that, the paste was deposited on an FTO glass substrate to fabricate photoanode films by the doctor-blade method. The films were annealed at the corresponding calcination temperature for 1 h to remove residual organic contamination. Then the films were bathed in an N3 dye ethanol solution with a molar concentration of 0.5 mM for 2 h at room temperature. Finally, the films were slightly rinsed with ethanol to remove any remaining dye. The photocathode consisted of an FTO glass coated with a platinum layer, and an electrolyte containing the triiodide/iodide (I_3^-/I^-) redox couple filled the space between the two electrodes. A sandwich-like structure of FTO–sample–FTO made up the photoelectrochemical cell. The cell was irradiated by simulated AM 1.5 sunlight with an output power of 100 mW cm^{-2} to characterize the photovoltaic behavior.

Table S1 Properties of the as-synthesized MMHO nanospheres.

Materials	**synthetic condition** (**[d] T1, [e] r**)	**[a] Pore size** (nm)	**[b] BET** ($m^2\ g^{-1}$)	**Langmuir Surface Area** ($m^2\ g^{-1}$)	**[c] Pore volume** ($cm^3\ g^{-1}$)
$Cu(OH)_2$-100	85 °C, r=0	2.4	414	592	0.64
$Cu(OH)_2$-150	85 °C, r=0.13	2.2	296	418	0.49
$Cu(OH)_2$-270	85 °C, r=0.15	2.7	287	377	0.35
$Zn(OH)_2$-100	85 °C, r=0	2.5	317	195	0.43
$Zn(OH)_2$-200	85 °C, r=0.10	2.6	249	351	0.27
$Fe(OH)_3$-100	85 °C, r=0	2.7	94	134	0.14
$Ni(OH)_2$-180	85 °C, r=0	2.4	177	247	0.30
Au@$Zn(OH)_2$	85 °C, r=0	2.2	60	82	0.18
Au@$Cu(OH)_2$	85 °C, r=0	2.4	418	577	0.40
$Zn_{0.15}Cu(OH)_{2.3}$	85 °C, r=0	2.5	308	440	0.61

[a] **Pore size** is calculated from adsorption branch of N_2 isotherm.

[b] **BET** is the BET surface area.

[c] **Pore volume** stands for the single point total pore volume determined by using the adsorption branch of the N_2 isotherm at $P/P_0 = 0.99$.

[d] T1 refers to the synthetic temperature.

[e] **r** refers to the ethanol/water volume ratio.

Table S2 Properties of the as-synthesized MMO nanospheres.

Materials	Treated temperature	[a] Pore size (nm)	[b] BET ($m^2 g^{-1}$)	Langmuir Surface Area ($m^2 g^{-1}$)	[c] Pore volume ($cm^3 g^{-1}$)
$Zn(OH)_2$-200-250°C	250 °C	2.4	159	237	0.36
$Zn_{0.15}CuO_{1.15}$-300°C	300 °C	6.0	35	50	0.17
Fe_2O_3-100-300°C	300 °C	2.3	153	227	0.13
ZnO-100-400°C	400 °C	9.1	41	57	0.24
ZnO-200-300°C	300 °C	6.3	97	140	0.20
ZnO-200-350°C	350 °C	7.6	54	75	0.15
ZnO-200-400°C	400 °C	11.0	37	52	0.16
ZnO-200-600°C	600 °C	18	39	54	0.31
$Cu(OH)_2$/CuO-100-200°C	200 °C	2.9	68	97	0.12
$Cu(OH)_2$/CuO-150-200°C	200 °C	2.8	119	169	0.25
$Cu(OH)_2$/CuO-270-200°C	200 °C	7.4	75	106	0.17
CuO-100-300°C	300 °C	11	16	24	0.07
NiO-180-300°C	300 °C	2.7	143	202	0.32
NiO-180-400°C	400 °C	3.4	73	103	0.23
Fe_2O_3-100-400°C	400 °C	7.6	23	32	0.16

ZnO-100-300°C	300 °C	4.8	145	209	0.43
ZnO-100-350°C	350 °C	6.9	66	93	0.32

[a] **Pore size** is calculated from adsorption branch of N_2 isotherm.

[b] **BET** is the BET surface area.

[c] **Pore volume** stands for the single point total pore volume determined by using the adsorption branch of the N_2 isotherm at $P/P_0 = 0.99$.

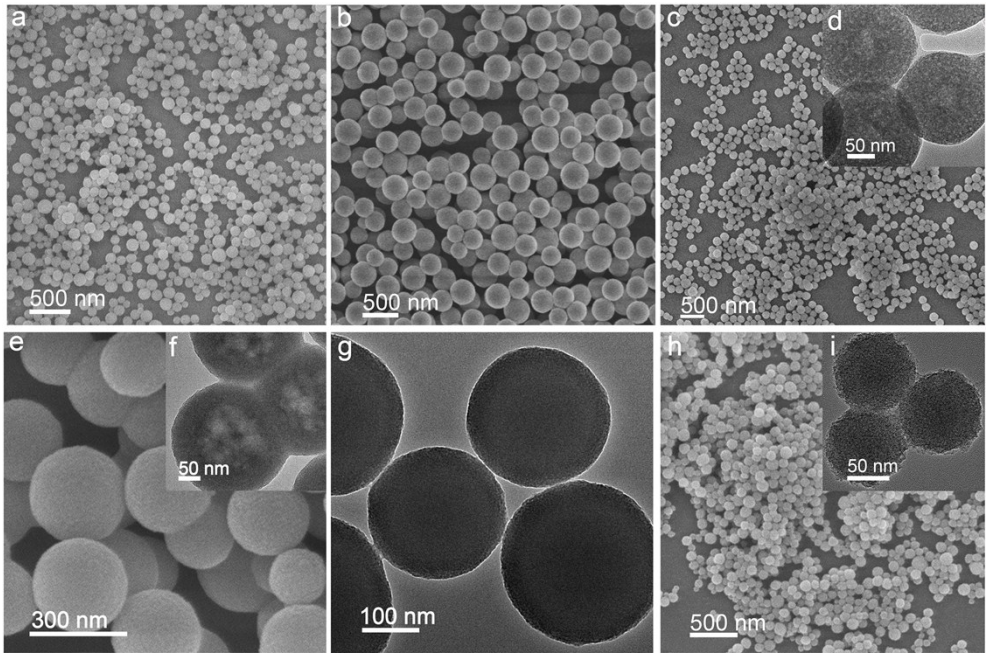

Fig. S1 SEM and TEM images of (a) $Cu(OH)_2$-100 nanospheres; (b) $Cu(OH)_2$-270 nanospheres; (c, d) $Zn(OH)_2$-200 nanospheres; (e, f) $Zn(OH)_2$-300 nanospheres; (g) $Ni(OH)_2$-280 nanospheres; (h, i) $Fe(OH)_3$-100 nanospheres.

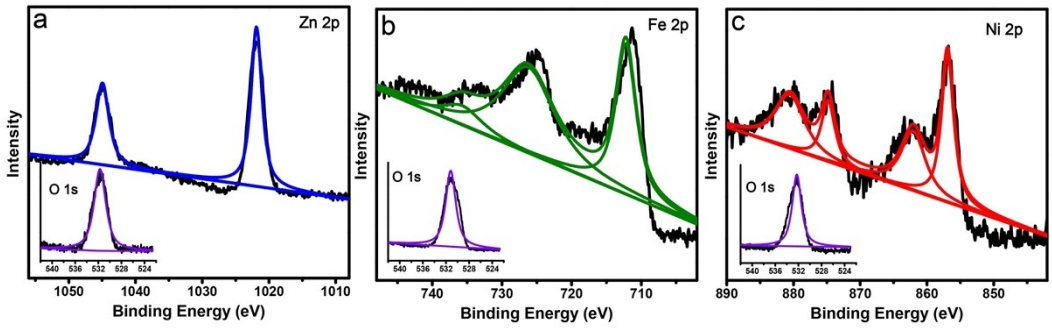

Fig. S2 XPS spectra of (a) $Zn(OH)_2$ nanospheres; (b) $Fe(OH)_3$ nanospheres; (c) $Ni(OH)_2$ nanospheres.

The growth process for the MMHO nanospheres was monitored using dynamic light scattering at certain time intervals (Fig. S3). The dynamic diameters of the reactants increased precipitously from ~5 to 62 nm after 2.5–3 h, in accordance with the nucleation of the nanospheres, and the nuclei of the nanospheres gradually grew to 92 nm as the reaction continued. Combining these results with the uniform and monodisperse characteristics of these spheres revealed by TEM and SEM, we concluded that the formation of nanospheres followed a nucleation-growth process.

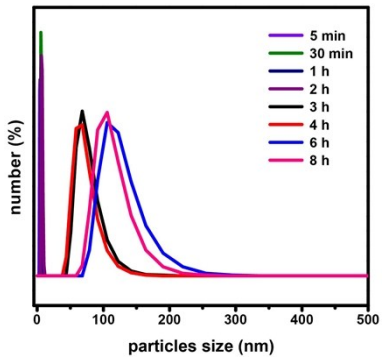

Fig. S3 Hydrodynamic diameters of $Zn(OH)_2$-100 nanospheres in the formation process.

Thermogravimetric analysis (TGA) in air showed the thermo-behaviors of representative samples before and after extraction with ufficient ethanol for enough time (Fig.S4a). All of the TGA curves behaved a weight loss between 25 ^oC and 700 ^oC and the largest weight-loss rates occur at 200-350 ^oC. $Cu(OH)_2$-100 was taken as an example, and the decomposition taking place in three stages has been shown. First step accompanied by 8.6% mass loss is between 100 oC and 200 ^oC, which is mainly related to the pyrolysis of $Cu(OH)_2$. Then, the mass loss between 200 ^oC and 420 oC is due to the decomposition of CTAB and the pyrolysis of $Cu(OH)_2$. The total mass loss was 51.8%, attributed to the pyrolysis of $Cu(OH)_2$ and the decomposition of CTAB. The mass loss of H_2O deriving from the pyrolysis of $Cu(OH)_2$ is calculated to be about 9.7% by evaluating the residual CuO from the TGA curve. Despite extracted with efficient ethanol in enough time, it revealed that the original $Cu(OH)_2$-100 behaved with a weight loss of 51.8% while template-extracted sample with a weight loss of 45.4%, which meant 85% of surfactant was left. As we calculated, the residual amounts of the surfactant are 85% for $Cu(OH)_2$, 83% for $Zn(OH)_2$, 71% for $Fe(OH)_3$, 81% for $Ni(OH)_2$, respectively.

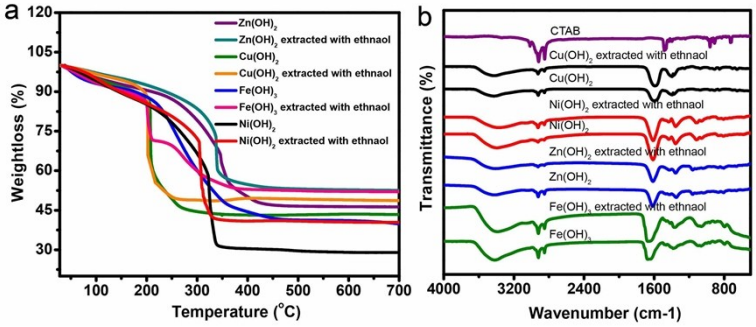

Fig. S4 (a) TG curves and (b) FTIR spectra of the as-synthesized MMHO nanospheres.

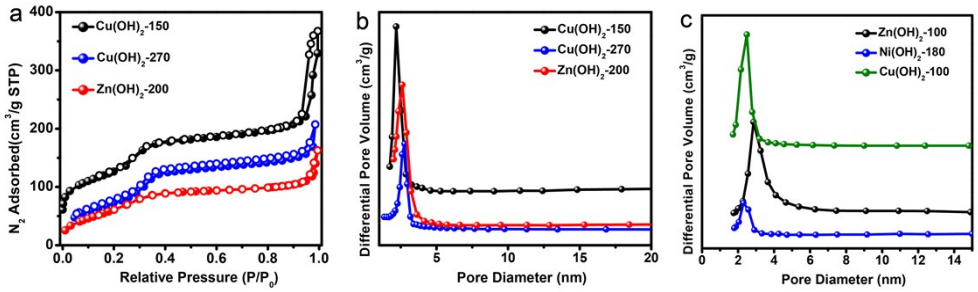

Fig. S5 (a) Nitrogen adsorption/desorption isotherms and (b, c) the corresponding pore size distribution of the as-synthesized MMHO nanospheres.

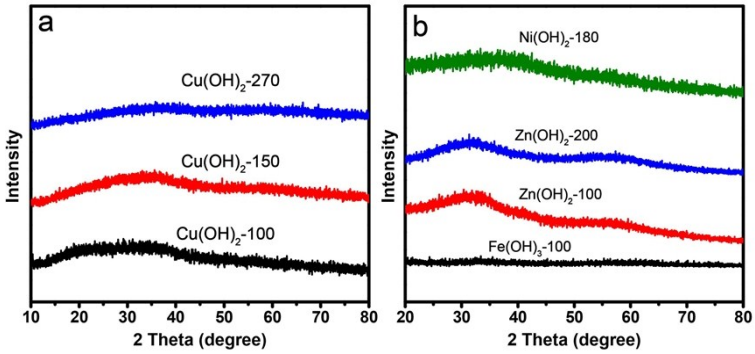

Fig. S6 (a, b) Power XRD patterns of amorphous MMHO nanospheres.

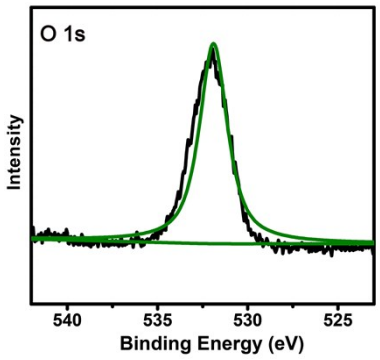

Fig. S7 O 1s XPS spectra of $Zn(OH)_2$-$Cu(OH)_2$ nanospheres with a molar ratio of Zn/Cu=0.15.

The wide-angle XRD patterns show the characteristic peaks of crystalline gold nanoparticles and amorphous peaks of acquired hydroxide shells (Fig.S8e), further confirming the successful encapsulation of gold nanoparticles. The N_2 adsorption-desorption isotherms of these two types of composited spheres gave typical-IV isotherms with high BET surface areas of 309 m^2/g for $Zn(OH)_2$-$Cu(OH)_2$ with a Zn/Cu molar ratio of 0.15, 418 m^2/g for Au@$Cu(OH)_2$, and 60 m^2/g for Au@$Zn(OH)_2$ nanospheres (Fig.S8f).

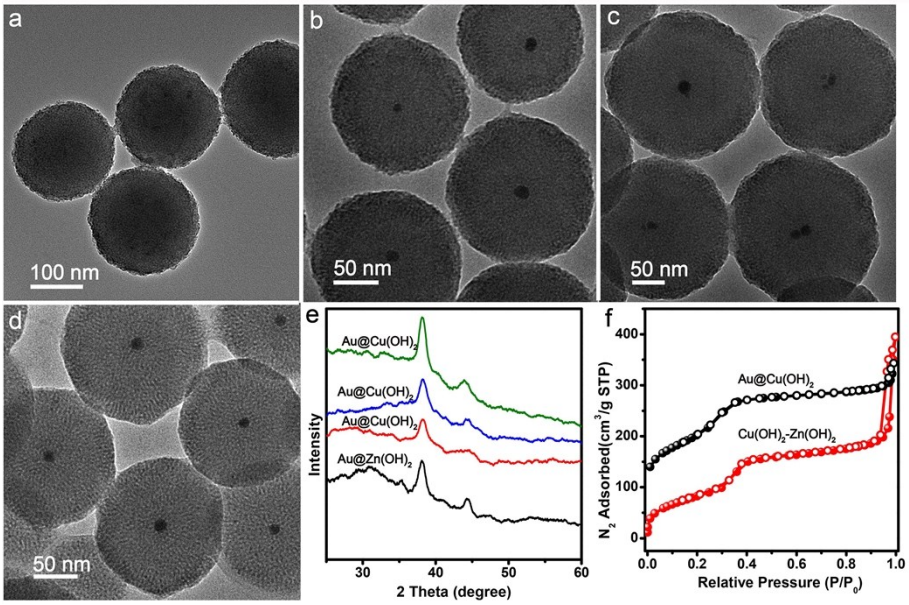

Fig. S8 TEM images of (a) $Zn(OH)_2$-$Cu(OH)_2$ nanospheres with the molar ratio of Zn/Cu=0.25; (b, c) Au@$Cu(OH)_2$ nanospheres; (d) Au@$Zn(OH)_2$ nanospheres. (e) Wide angel XRD patterns and (f) nitrogen adsorption/desorption isotherms of Au@$Zn(OH)_2$, $Cu(OH)_2$-$Zn(OH)_2$ and Au@$Cu(OH)_2$ nanospheres.

Mesoporous $Cu(OH)_2$ nanospheres directly pyrolyzed into CuO at 300°C, and complexation of $Cu(OH)_2$ and CuO occurred at 200°C (Fig. S9a-c).

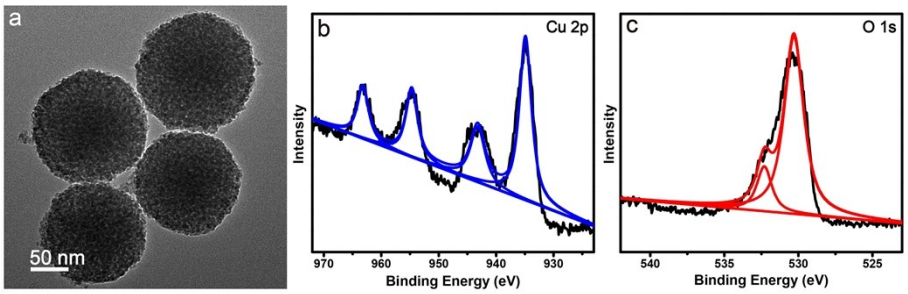

Fig. S9 (a) TEM image and (b, c) XPS spectra of $Cu(OH)_2$ nanospheres calcined at 200°C.

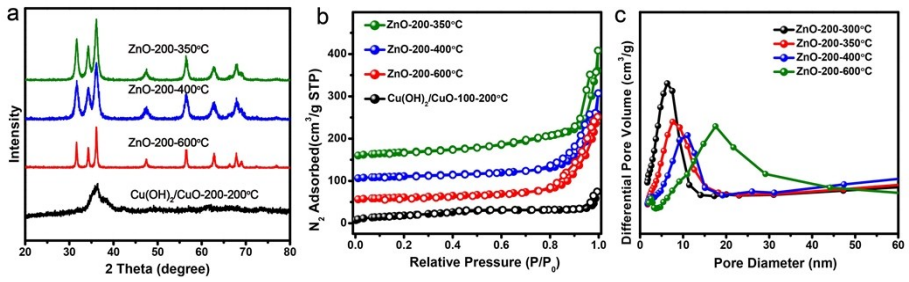

Fig. S10 (a) XRD patterns, (b) nitrogen adsorption/desorption isotherms and (c) pore size distribution curves of MMHO nanospheres calcined at different temperatures.

Table S3 Comparison of OER activity of the calcined $Cu(OH)_2$ with reported Cu-based catalysts.

Electrode	Overpotential@10 mA cm^{-2} (mV)	Ref.
$Cu(OH)_2$/CuO-100-200°C	410	This work
CuO from Cu-EA	475	*Chem. Commun.*, 2016, **52**, 5546-5549
Cu-CMP850	475	*ChemSusChem*, 2016, **9**, 2365 – 2373
O_2-Cu-TPA	*	*ACS Catal.*, 2015, **5**, 1530–1538.
annealed CuO	580	*J. Phys. Chem. C*, 2016, **120**, 831–840.
$NiCuO_x$	*	*J. Mater. Chem. A*, 2017, **5**, 4331
nanostructured Cu oxide	290	*Angew. Chem. Int. Ed.* 2017, **56**, 4792-4796

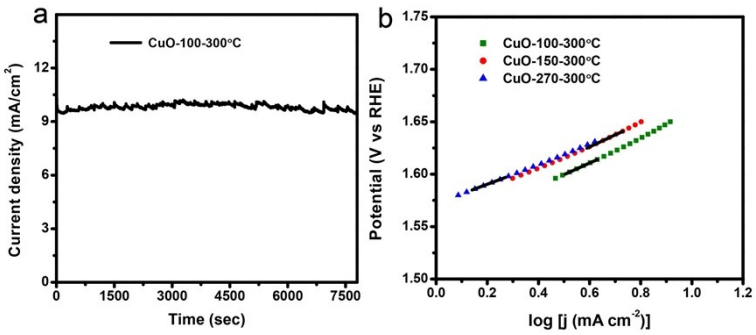

Fig. S11 (a) Catalytic overpotential plot using the active CuO nanospheres under static current density of 10 mA cm^{-2} in 1.0 M KOH solution and (b) tafel plots of the mesoporous $Cu(OH)_2$ nanospheres calcined at 300°C.

References

1. Z. Dong, X. Lai, J. E. Halpert, N. Yang, L. Yi, J. Zhai, D. Wang, Z. Tang and L. Jiang, *Adv. Mater.*, 2012, **24**, 1046.